

## Article

# Second-Life Assessment of Commercial LiFePO<sub>4</sub> Batteries Retired from EVs

Zhi Cao <sup>1</sup>, Wei Gao <sup>1</sup>, Yuhong Fu <sup>1</sup>, Christopher Turchiano <sup>2</sup>, Naser Vosoughi Kurdkandi <sup>1</sup>, Jing Gu <sup>2</sup> and Chris Mi <sup>1,\*</sup>

<sup>1</sup> Department of Electrical and Computer Engineering, San Diego State University, San Diego, CA 92182, USA; zcao2@sdsu.edu (Z.C.); wgao2@sdsu.edu (W.G.); yfu@sdsu.edu (Y.F.); nvosoughikurdkandi@sdsu.edu (N.V.K.)

<sup>2</sup> Department of Chemistry and Biochemistry, San Diego State University, San Diego, CA 92182, USA; cturchiano1590@sdsu.edu (C.T.); jgu@sdsu.edu (J.G.)

\* Correspondence: cmi@sdsu.edu

**Abstract:** LiFePO<sub>4</sub> (LFP) batteries are well known for their long cycle life. However, there are many reports of significant capacity degradation in LFP battery packs after only three to five years of operation. This study assesses the second-life potential of commercial LFP batteries retired from electric vehicles (EVs) by evaluating their aging characteristics at the cell and module levels. Four LFP cells and four modules were subjected to aging tests under various conditions. The results indicate that LFP cells exhibit long life cycles with gradual capacity degradation and a minimal internal resistance increase. Module-level analysis reveals significant balance issues impacting capacity recovery. Incremental capacity analysis (ICA) and post-mortem analysis identify the loss of active materials and lithium inventory as key aging mechanisms. This study provides the optimal working conditions of second-life LFP batteries and suggests that, with proper balancing systems, LFP batteries can achieve extended second-life use in stationary energy storage applications, emphasizing the importance of effective balance management for sustainable battery utilization.

**Keywords:** LFP battery; second-life battery; echelon utilization; battery balance; battery aging



**Citation:** Cao, Z.; Gao, W.; Fu, Y.; Turchiano, C.; Vosoughi Kurdkandi, N.; Gu, J.; Mi, C. Second-Life Assessment of Commercial LiFePO<sub>4</sub> Batteries Retired from EVs. *Batteries* **2024**, *10*, 306. <https://doi.org/10.3390/batteries10090306>

Academic Editor: Ottorino Veneri

Received: 30 July 2024

Revised: 21 August 2024

Accepted: 27 August 2024

Published: 30 August 2024



**Copyright:** © 2024 by the authors. Licensee MDPI, Basel, Switzerland. This article is an open access article distributed under the terms and conditions of the Creative Commons Attribution (CC BY) license (<https://creativecommons.org/licenses/by/4.0/>).

## 1. Introduction

The adoption of electric vehicles (EVs) has surged in recent years. In 2023, over 14 million EVs and plug-in hybrid vehicles (PHEVs) were sold worldwide, capturing 16% of the total vehicle market. Predictions indicate that EV and PHEV sales will reach 60 million units by 2035 [1]. Consequently, tens of millions of EV battery packs, totaling hundreds of gigawatt-hours, will be decommissioned annually after serving 8 to 15 years [2–4]. Utilizing these retired batteries for second-life applications is considered the most cost-effective and environmentally sustainable option compared to direct material recycling [5,6].

LiFePO<sub>4</sub> (LFP) batteries are widely used for EV and battery energy storage system (BESS) applications due to their high-power capabilities [7], low fire risks [8], low cost, and long cycle life [9]. Compared to Li-NCM batteries, which suffer from aging knee issues [10,11], LFP batteries' capacity fading is generally mild, following an approximately linear pattern at room temperature [12], and the positive electrodes usually do not exhibit a significant decline under moderate ambient temperatures [13].

Various studies have investigated LFP batteries. In ref. [14], a cycle aging study on a commercial LFP cell investigated the influence of the temperature, C-rate, depth of discharge (DoD), and state of charge (SoC) on the capacity and impedance degradation. The findings highlighted the significant impact of the DoD and SoC in terms of capacity reduction and a resistance increase, while the C-rate had a minimal effect. Some works have studied the aging mechanisms of LFP batteries [15,16]. Jiang et al. [17] used incremental capacity analysis (ICA) and IC peak area analysis to identify the aging modes. They found

a consistent aging pattern across all batteries studied, characterized by a loss of lithium inventory and active materials on the negative electrodes. Some post-mortem analyses have been conducted to further verify the aging mechanisms of LFP batteries [18]. In ref. [19], macroscopic and microscopic techniques were used to identify the aging phenomenon occurring in the cell on the positive and negative electrodes. The results showed a stable positive LFP electrode but significant deposits and cracking on the negative electrode. Zhu et al. [20] investigated commercial 100 Ah prismatic graphite/LiFePO<sub>4</sub> batteries cycled under 45 °C and found that electrolyte loss due to the enhanced evolution of the solid electrolyte interface (SEI) film resulted in the loss of the lithium inventory. They observed that larger LFP particles are prone to fracturing and that Fe deposition accelerates SEI film formation, which blocks graphite layers and impedes lithium intercalation.

Despite the long life cycles of LFP batteries at the cell level, there have been many reports of LFP battery packs in EVs or BESSs retiring earlier than expected, usually due to balance issues [21,22]. Ramirez-Meyers et al. [22] found significant variations and mismatches in the SoH within the modules of used HEV packs, rendering them unsuitable for reuse. Jiang et al. [23] discovered that LFP battery module parameter dispersion increases with battery aging, and SoC imbalance is the main factor contributing to capacity fading in the battery pack.

To study retired LFP batteries and evaluate their second-life value, a study is carried out at both the cell and module levels. The aging characteristics of LFP battery cells under various working conditions are investigated, and the aging mechanisms are revealed by different methods. The health conditions of LFP battery modules are analyzed in terms of their capacity, impedance, balance state, and consistency. Based on the analysis, we provide a comprehensive evaluation of the second-life use of LFP batteries and clarify the prospects for the second-life utilization of LFP batteries with a proper balance system.

The remainder of this paper is organized as follows. In Section 2, the battery cell and module test are introduced. Section 3 analyzes the battery cell aging characteristics, module health conditions, second-life evaluation, recommended second-life working conditions, etc. In Section 4, the battery post-mortem analysis is demonstrated. Conclusions are drawn in Section 5.

## 2. Experimental Description

### 2.1. Description of Experimental Procedures with LFP Battery Cells

This study utilizes LFP battery cells manufactured by China Aviation Lithium Battery Co., Ltd. (CALB, Luoyang, China). The main specifications of the CALB LFP batteries are detailed in Table 1 [24]. Four battery cells were collected for this study, and their initial conditions are summarized in Table 2. Cells 01 and 02 were new. According to initial tests, the actual capacity of the new cells was 107 Ah, which was used as the nominal capacity instead of the labeled 100 Ah. Cells 03 and 04 were retired from electric forklifts after four years of service.

**Table 1.** Specifications of the CALB LFP batteries.

Parameter	Value
Nominal Capacity	100 Ah @ 0.3 C
Nominal Voltage	3.2 V
Charge (CC-CV)	1 C/3.65 V
Charging Time	Standard: 4 h Quick charging: 1 h
Discharge	2 C/2.5 V
Recommended SoC Window	10–90%
Charge Temperature	0–45 °C
Discharge Temperature	0–55 °C
Internal Resistance	≤0.9 mΩ
Weight	3.4 kg
Cell Packaging Type	Prismatic
Dimensions	142 mm × 67 mm × 219 mm
Energy Density	100 Wh/kg

**Table 2.** Initial conditions and test dates of CALB LFP battery cells.

Cell Number	Initial Capacity (Ah)	SoC	Initial Capacity Test Date	Cycling Test Start Date
Cell 01	107.2	100.2%	July 2020	September 2020
Cell 02	107.1	100.1%		March 2022
Cell 03	95.0	88.8%		September 2020
Cell 04	94.6	88.4%		September 2020

The battery test system shown in Figure 1 was used to conduct accelerated cycling tests on the LFP batteries. A Chroma 17010 battery cell tester, with 24 channels, was employed for the battery aging experiments. Each channel operated within a voltage range of 0 V to 5 V, with a maximum current capacity of 100 A. For testing under varying temperature conditions, a CSZ Plus 8 chamber was used for high temperatures, while a THERMOTRON thermal chamber was utilized for low-temperature tests.

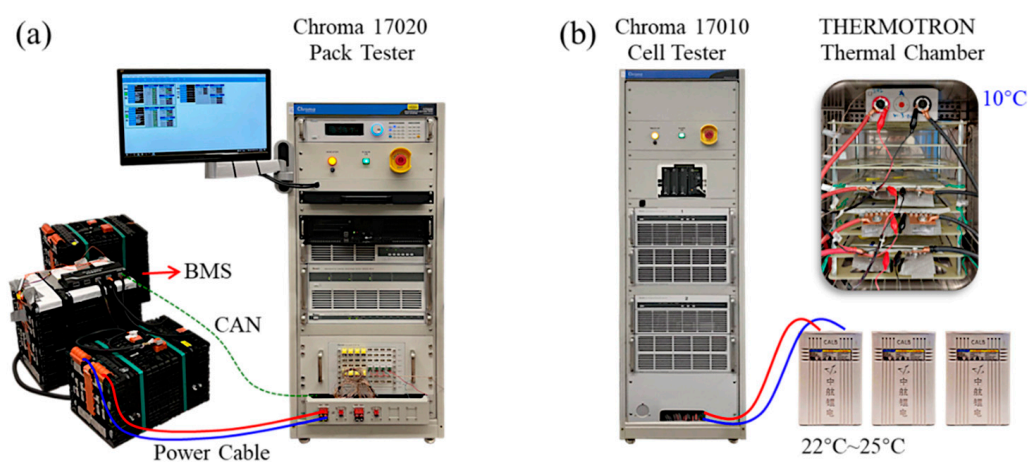


**Figure 1.** Battery test system: (a) battery pack tester; (b) The Chinese characters (中航锂电) in the figure stand for CALB.

To study the aging characteristics of the LFP batteries during second-life use, the working voltage range was downscaled from 2.0 V~3.65 V to 2.8 V~3.60 V. The aging tests were divided into different groups, each with different working conditions. In the initial stage, all battery cells were cycled between 3.10 V and 3.45 V. The charge current was 60 A, and the discharge current was 95 to 100 A. In the following stages, the cycling range was adjusted to different levels, such as 2.80 V to 3.45 V, 2.80 V to 3.60 V, etc. The current was also varied in the different stages to study its effect on battery degradation. All battery cells were tested at room temperature (23 °C), except Cell 03, which was tested at a high temperature for some time. The test conditions used in the aging tests were selected based on common operating conditions for LFP batteries in electric vehicles and energy storage systems. The cycling test start dates for all battery cells are given in Table 2. Cell 02 rested for 1.5 years before the cycling aging test.

Figure 2 presents the aging test data for Cell 03 across various stages. Each stage included 55 aging cycles under specific conditions, followed by 5 characteristic test cycles, which were used to assess the battery capacity and impedance. Data during cycling were captured at 5 s intervals. The characteristic tests, performed at room temperature, consisted of a 0.2 C capacity test, two 0.5 C capacity tests, and a hybrid pulse power characterization (HPPC) test to determine the battery impedance. When aging cycles occurred at high temperatures, the thermal chamber was set to 23 °C and allowed to stabilize for eight hours before conducting the characteristic tests. The test conditions remained consistent within each stage to ensure the reliable evaluation of the battery parameters but were adjusted between stages to account for significant changes in capacity and impedance. The

0.2 C capacity from 2.80 V to 3.55 V was considered the cell’s capacity, and the HPPC test data were recorded at 1 s intervals for the battery parameter analysis.

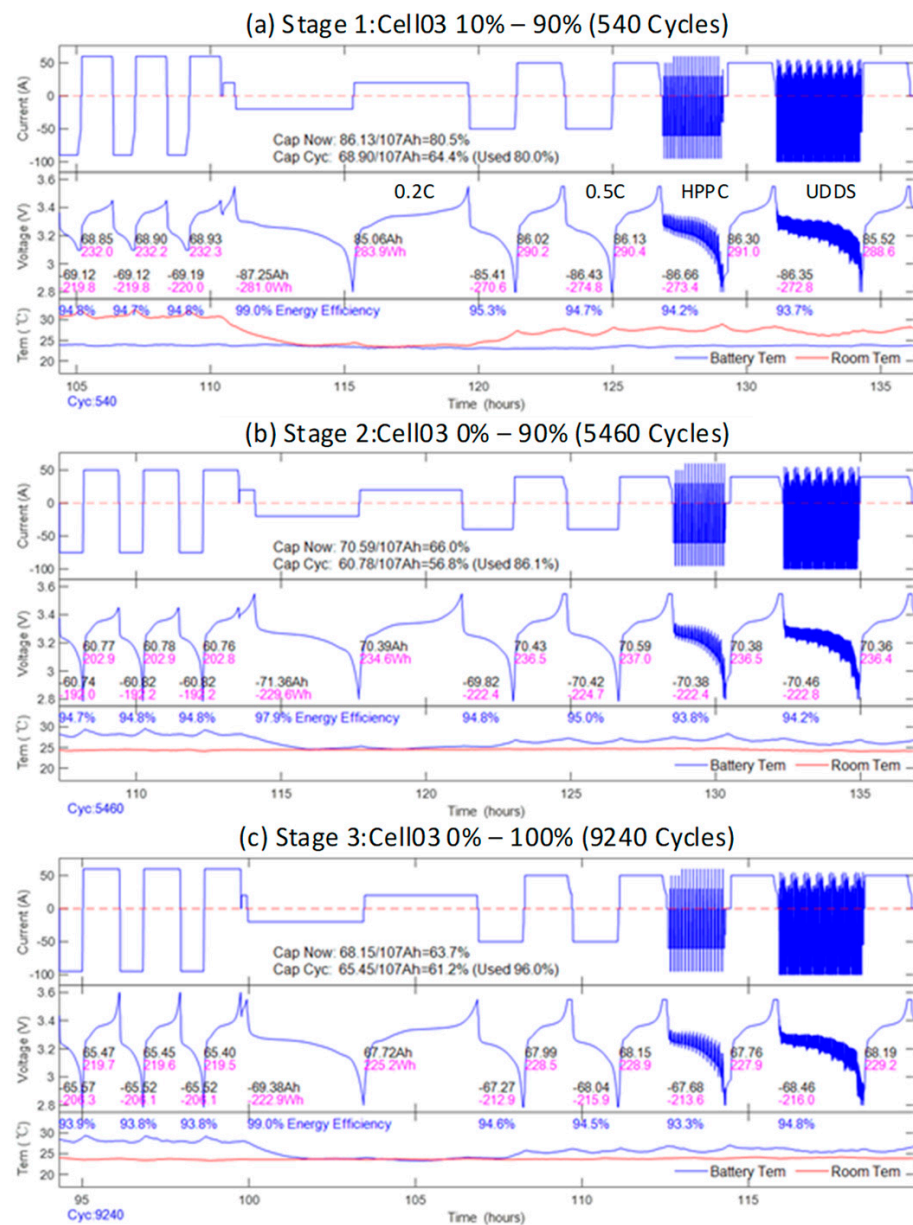


**Figure 2.** CALB battery cell aging test data. (a) Cell 03 after 540 cycles; (b) Cell 03 after 5460 cycles; (c) Cell 03 after 9240 cycles.

### 2.2. Description of Experimental Procedures with LFP Battery Modules

The LFP battery modules used in this study were sourced from BYD. Four retired battery modules were collected for the study. After around four to five years of service in California, USA, these battery modules were retired from BYD K9M electric buses. Modules 01 and 02 came from the same vehicle, with a configuration of 1P12S. Modules 03 and 04 were from another vehicle, with a configuration of 1P8S. The main specifications of the BYD LFP batteries are detailed in Table 3.

**Table 3.** Specifications of the BYD LFP batteries.

Parameter	Value
Nominal Capacity	270 Ah
Voltage Range	2.8–3.8 V (3.2 V Nominal)
Module Weight	59.5 kg
Cell Packaging Type	Prismatic
Dimensions	415 mm × 60 mm × 145 mm
Energy Density	116 Wh/kg
Charge Current	Standard: 100 A; Max: 200 A @25 °C
Discharge Current	Standard: 200 A

To evaluate the SoH of the retired BYD battery modules in terms of the module capacity, cell capacity distribution, and internal resistance, the following tests were designed.

- (1) A battery module test system was used to test the battery modules and obtain their capacities. The internal resistances of the cells were calculated afterward.
- (2) A battery cell tester was used to obtain the cells' capacities within the module. Then, all cells were fully charged to have the modules achieve a top-balanced state.
- (3) The modules' capacities were tested again after balancing.

The battery cell test system was the same as the one used for the CALB cell testing. The module test system, shown in Figure 1, consisted of a Chroma 62024P-80-60 DC power supply, a Chroma 63203 DC electric load, a dSpace AutoBox as the main controller, and a BMS to measure the battery cell voltage and temperatures.

### 2.3. Battery Impedance Calculation

The 1-RC equivalent circuit model was applied to calculate the battery parameters [25,26]. This model comprises a voltage source represented by an open circuit voltage (OCV)–Ah curve, along with an ohmic resistance  $R_0$  and an RC network that includes diffusion resistance  $R_1$  and capacitor  $C_1$ . The battery impedance is characterized by the parameters  $R_0$  and  $R_1$ . The 1-RC model is structured as follows:

$$\begin{cases} \dot{U}_1 = -\frac{1}{R_1 C_1} U_1 + \frac{1}{C_1} I_t \\ U_t = U_{OC} - U_1 - I_t R_0 \end{cases} \quad (1)$$

where  $U_1$  represents the voltage across the RC network,  $I_t$  denotes the load current,  $U_{OC}$  is the OCV, and  $U_t$  refers to the terminal voltage. Its discrete-time format can be expressed as

$$\begin{cases} U_{1,k+1} = \exp(-\Delta t / R_1 C_1) \times U_{1,k} + [1 - \exp(-\Delta t / R_1 C_1)] \times I_{t,k} R_1 \\ U_t = U_{OC} - U_1 - I_t R_0 \\ D_1 = \exp(-\Delta t / R_1 C_1) \end{cases} \quad (2)$$

where  $k$  indicates the step,  $\Delta t$  represents the time interval (1 s in this study),  $U_{1,k+1}$  is the voltage  $U_1$  at time step  $k + 1$ ,  $I_{t,k}$  is the current  $I_t$  at time step  $k$ , and  $D_1$  is the time constant.

The model input is  $I_t$  while the output is  $U_t$ . Both the input and output are measurable in the physical system. The parameters  $U_{OC}$ ,  $R_0$ ,  $R_1$ , and  $D_1$  are unknown. The particle swarm optimization (PSO) algorithm is employed to estimate these parameters using the HPPC data. The specifics of the algorithm are detailed in references [10,27] and not repeated here.

## 3. Results and Discussion

### 3.1. CALB Battery Cell Aging Test Results

#### 3.1.1. Aging Speed Analysis

Figure 3a–d present the aging trajectories of Cells 01 to 04, including the capacity and internal resistance versus test cycles and full equivalent cycles (FECs). The FEC is defined as the total discharge throughput capacity scaled by the battery's nominal capacity. Retired

Cells 03 and 04 have completed over 11,000 test cycles under varying conditions, with average aging rates of 3.41% and 2.56% per 1000 cycles, respectively. This is equivalent to 32 years of actual operation at one cycle a day. In terms of the FECs, Cells 03 and 04 could complete 7000 cycles. New Cell 01 lost 33.3% of its capacity after 10,390 cycles (8000 FECs), with an average aging rate of 3.275% per 1000 cycles, while Cell 02 lost 19.83% of its capacity within 4510 cycles, with the highest aging rate of 4.397% per 1000 cycles. The initial and final capacities of the four cells are summarized in Table 4. It is evident that LFP battery cells have very long life cycles.

**Table 4.** Battery cell statistics at the start and end of the aging tests.

Cell Number	01	02	03	04
Initial capacity (Ah)	107.1 (100%)	104.48 (97.64%)	95.0 (88.79%)	94.6 (88.41%)
Final capacity (Ah)	70.69 (66.7%)	83.26 (77.81%)	51.45 (48.08%)	62.53 (58.44%)
Testing cycles	10,390	4510	11,930	11,710
Average aging speed per 1000 cycles	3.275%	4.397%	3.412%	2.560%

Battery Cells 03 and 04 operated for four years before retiring. The estimated first-life cycle count was 1200. Based on their capacity at retirement, the estimated aging rate during first-life use was 9.58% per 1000 cycles. In the aging test, new Cells 01 and 02 were cycled under conditions that mimicked the first-life use of Cells 03 and 04. Their capacity degraded to the initial capacity of Cells 03 and 04 after approximately 1400 cycles. The first-life aging rate in the laboratory test was similar to that in real-world conditions.

Figure 4 presents the working conditions and aging speeds during the aging cycling tests. It is observed that the aging speed is faster at the beginning of the test and then slows down gradually. For example, the aging speed of Cell 01 decreases significantly after 3000 cycles. Even though the discharge cutoff voltage decreases from 3.10 V to 2.80 V during this period, the aging speed does not change. However, a lower discharge cutoff voltage, such as 2.6 V between 5100 and 5700 cycles and 2.5 V between 8400 and 8760 cycles, causes a slight increase in the aging speed. However, increasing the charge cutoff voltage within 3.60 V does not contribute to an accelerated aging speed. Similar aging behaviors are observed in Cells 03 and 04. After 3840 cycles, although the discharge cutoff voltage of Cell 3 decreases from 3.10 V to 2.80 V, the aging speed remains near zero. However, a lower discharge cutoff voltage, such as 2.60 V from 6420 to 7080 cycles and 2.0 V from 10,030 to 10,570 cycles, raises the aging speed. The effect of the charge and discharge current on the aging speed is less evident from the testing results. The testing temperature for Cells 01, 02, and 04 was always 23 °C, while the temperature of Cell 03 was raised from 45 °C to 55 °C between 9680 and 10,160 cycles. The high temperature caused a increase in the aging speed (about 15.5% per 1000 cycles), after which an aging knee occurred. Cells 03 and 04 degraded faster when their capacity dropped to 65% of the nominal capacity after about 10,000 aging cycles. Even with the cycling current reduced to 30 A, the trend did not change.

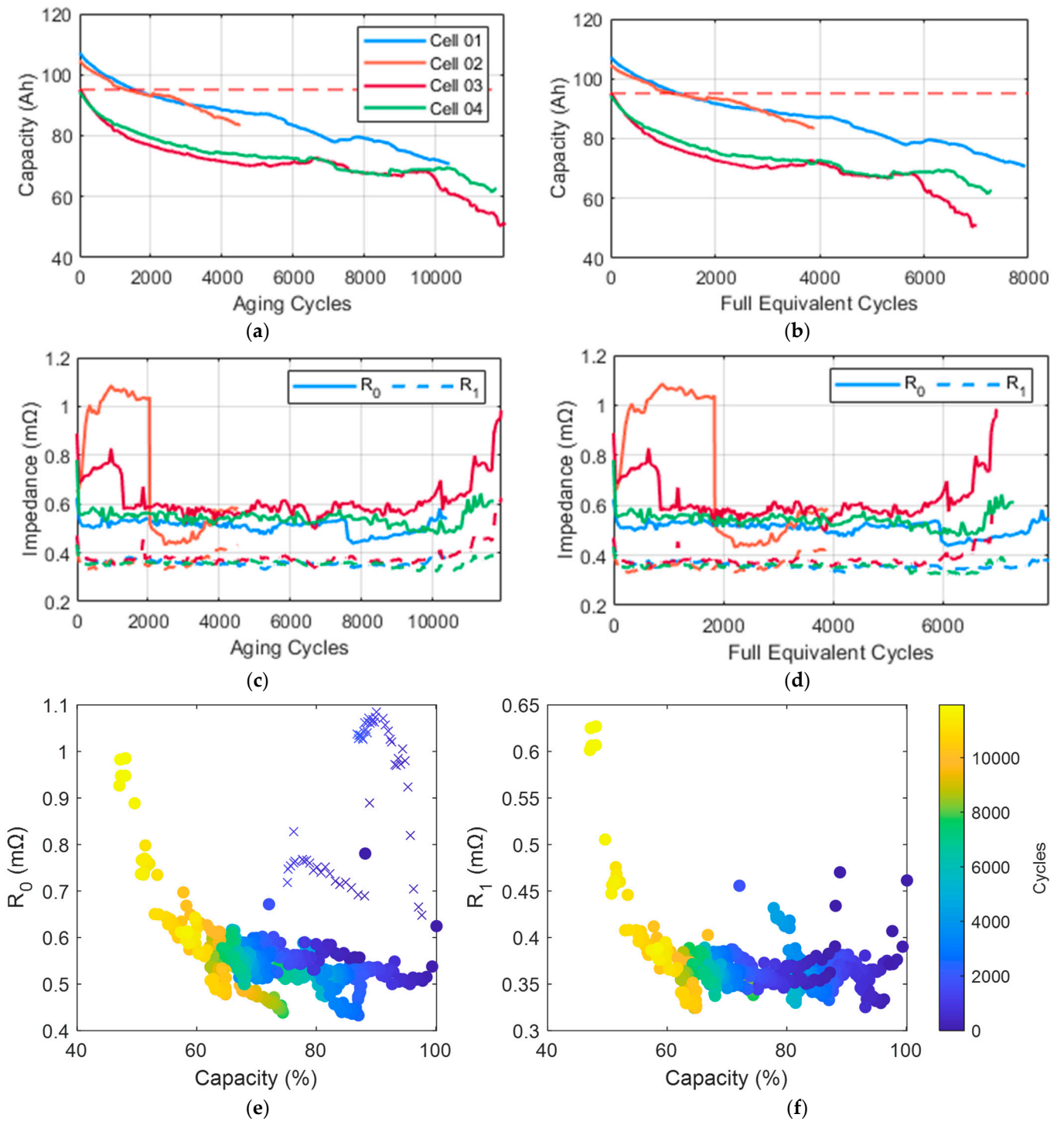


**Figure 3.** Battery aging test results: (a) capacity trajectories versus test cycles; (b) capacity trajectories versus full equivalent cycles; (c) internal resistance trajectories versus test cycles; (d) internal resistance trajectories versus full equivalent cycles. (e) Correlation between capacity and internal resistance  $R_0$  (The cross represents the abnormalities of Cells 02 and 03 in the first 1000 to 2000 cycles.); (f) correlation between capacity and internal resistance  $R_1$ . The dotted lines in (a,b) indicate the initial capacity level of retired Cells 03 and 04. The solid line in (c,d) are the internal resistance  $R_0$  while the dotted line in (c,d) represents  $R_1$ .

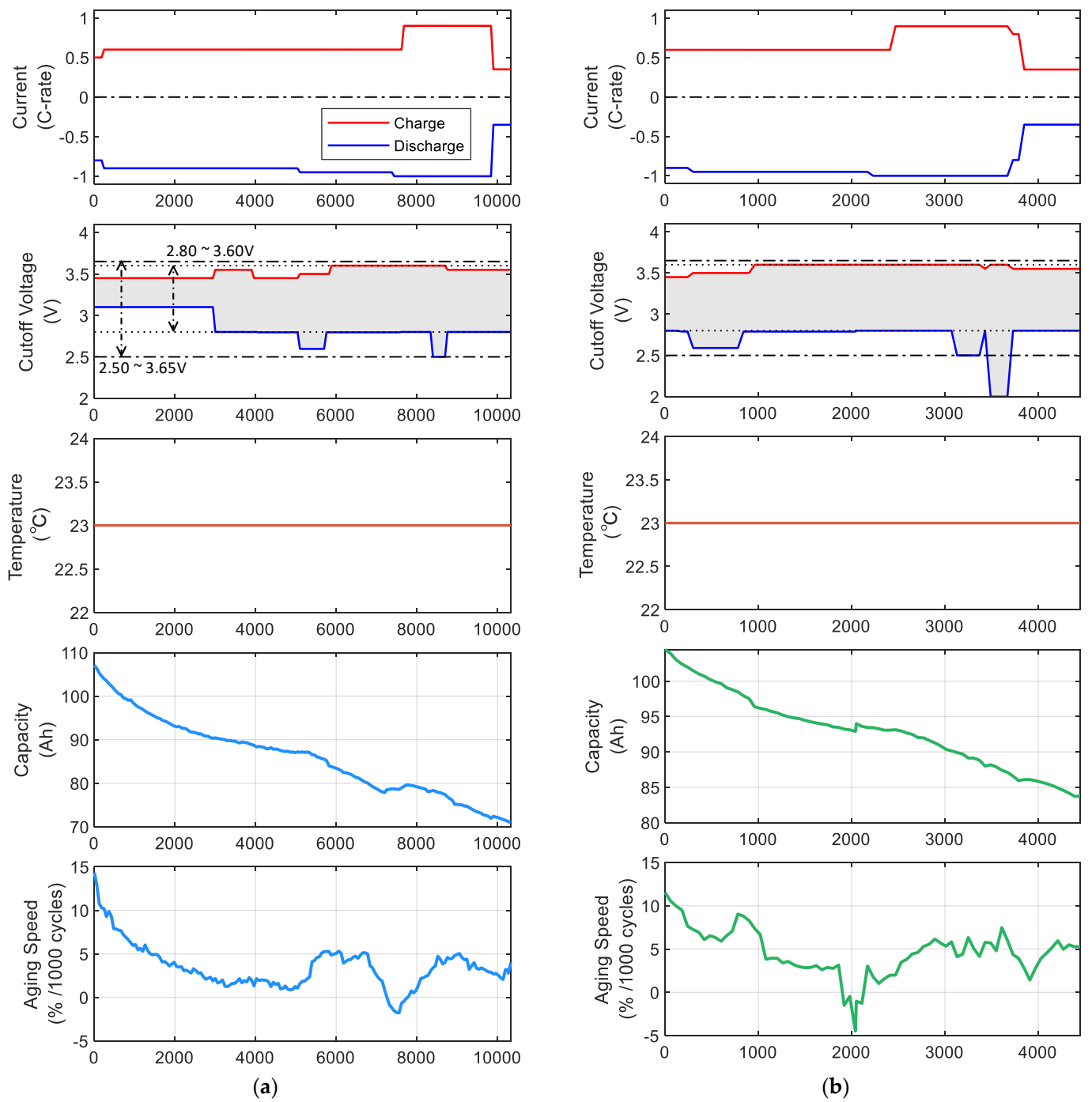
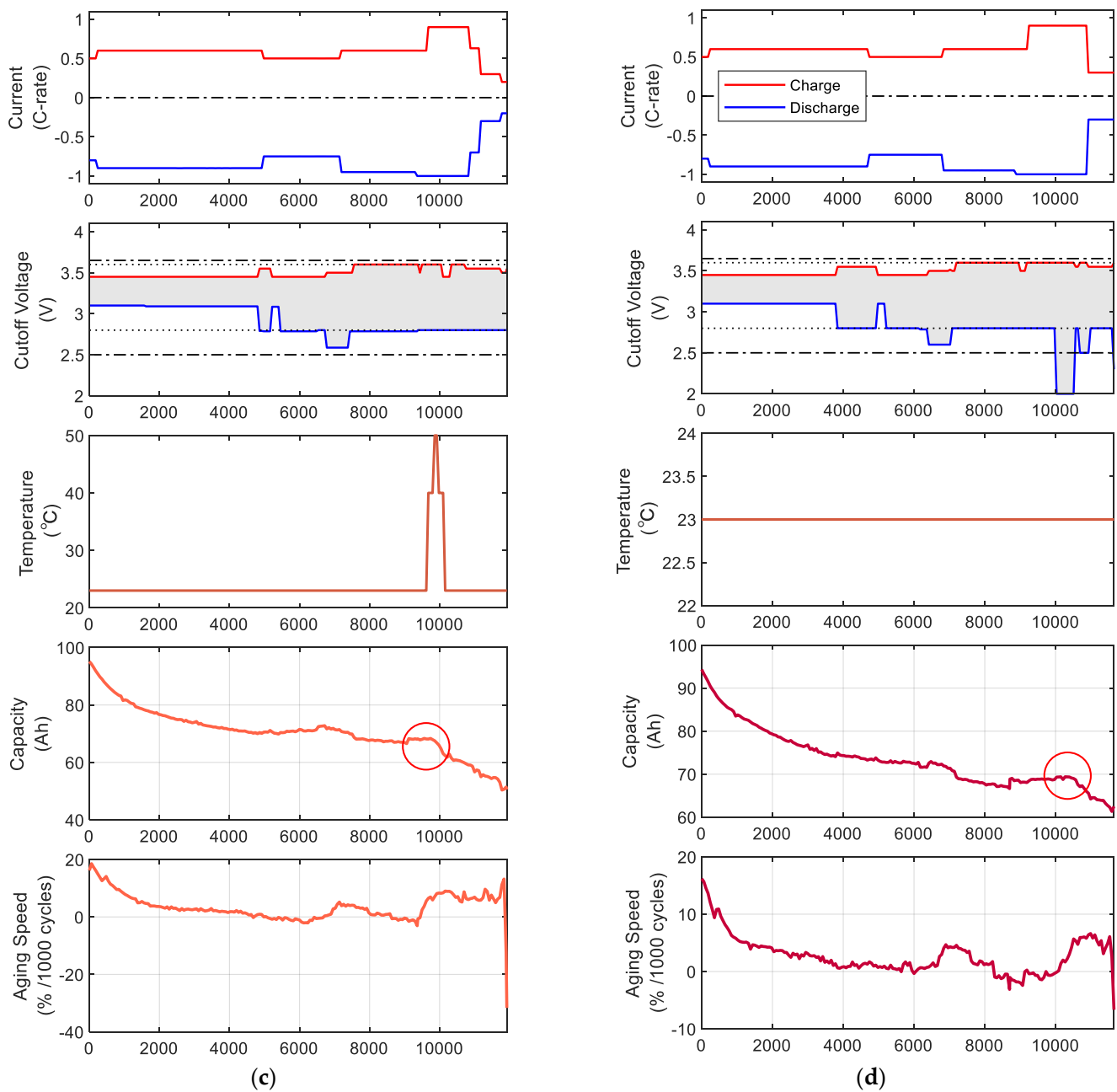


Figure 4. Cont.



**Figure 4.** Battery cycling conditions, capacity trajectories, and aging speeds: (a) Cell 01, (b) Cell 02, (c) Cell 03, (d) Cell 04.

### 3.1.2. Internal Resistance Analysis

The internal resistance of the battery cells remains consistently low over 10,000 cycles.  $R_0$  ranges between 0.5 m $\Omega$  and 0.6 m $\Omega$ , and  $R_1$  is around 0.36 m $\Omega$ . The internal resistance starts to increase after 10,000 cycles. The internal resistances of Cells 02 and 03 show an abnormal increase in the first 1000 to 2000 cycles and return to normal levels afterward. Figure 3e,f show the correlation between the impedance and capacity. The impedances of the batteries do not show a noticeable increase until 60% SoH. After this, the battery impedance increases drastically with the capacity degradation. The cross marks in Figure 3e indicate the abnormalities of Cells 02 and 03 in the first 1000 to 2000 cycles.

Low internal resistance ensures good power performance. CALB LFP batteries have Coulomb efficiency of nearly 100%, and the round-trip energy efficiency is about 94% to 95% at 0.6 C charging and 1 C discharge currents. The energy efficiency can be increased

to 98% at a 0.2 C current. The energy efficiency does not change across 10,000 aging cycles because of the lack of increase in the internal resistance.

### 3.1.3. Incremental Capacity Analysis (ICA) to Identify Aging Modes

Incremental capacity analysis (ICA) is a useful tool in identifying battery degradation modes [28,29]. Figure 5 illustrates the  $dQ/dV$  curves for Cells 01, 02, and 03, where three distinct peaks are visible. The changes in the intensity and position of these peaks suggest different degradation mechanisms, such as the loss of lithium inventory (LLI), loss of active material (LAM) at the negative electrode (NE), and LAM at the positive electrode (PE) [30,31].

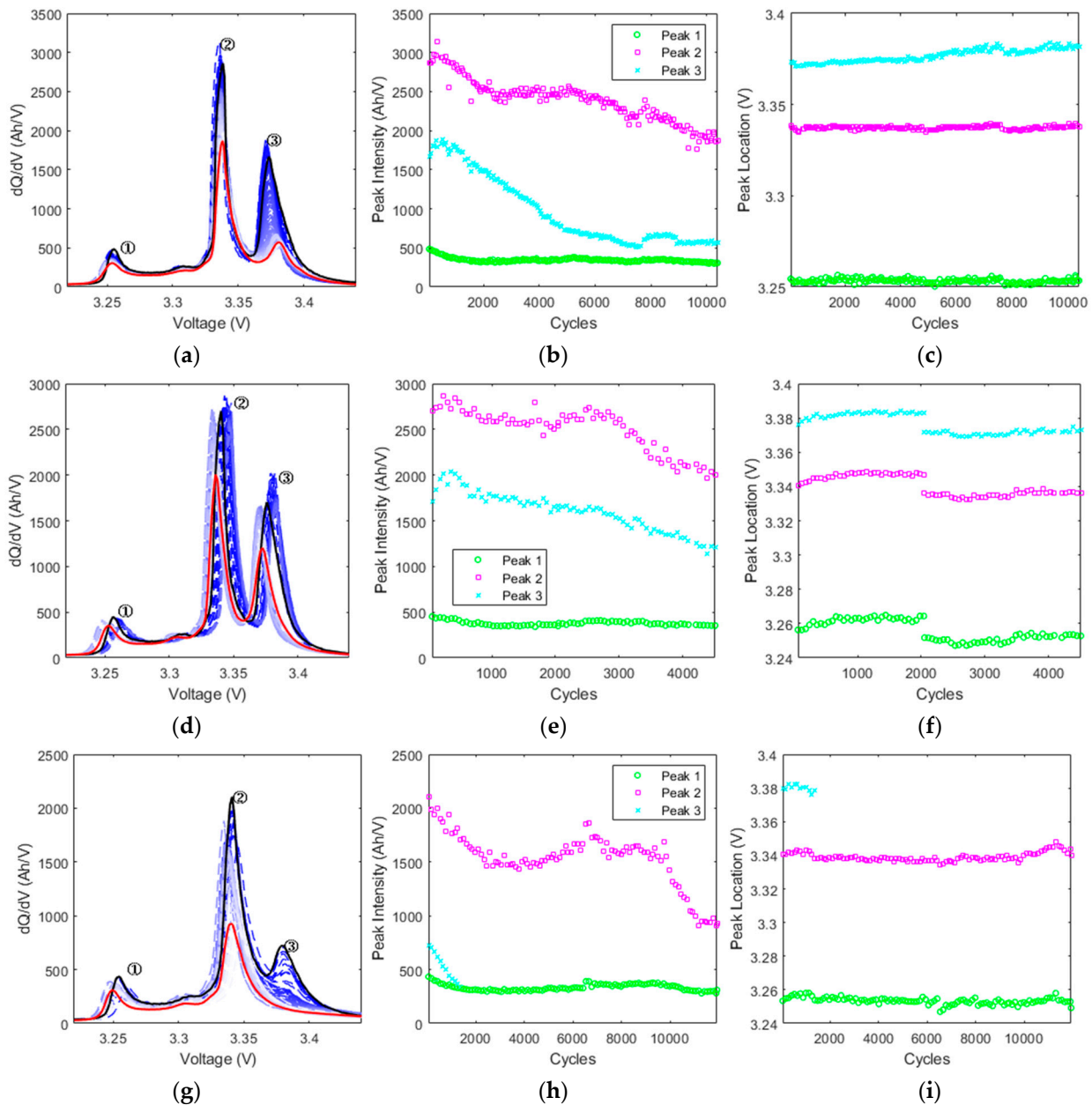


**Figure 5.** ICA analysis: (a,d,g)  $dQ/dV$  curves of battery Cells 01, 02, and 03 (black curves represent the start cycle, red curves represent the end cycle, and blue curves fade as the number of cycles increases). (b,e,h) Peak intensities versus cycle numbers for Cells 01, 02, and 03. (c,f,i) Peak positions versus cycle numbers for Cells 01, 02, and 03.

For new Cells 01 and 02, Peaks 1 and 2 decrease monotonously throughout cycling, implying that a combination of LAM at the NE and LLI causes the capacity to fade. The intensity of Peak 3 grows to a maximum in the first 400 to 500 cycles and then drops rapidly in a linear manner. This is because the LAM at the NE makes the excess relative capacity of the NE available for intercalation [32]. As the LAM at the NE increases, the NE eventually reaches a point where its relative capacity is entirely within the range of the PE. Consequently, Peak 3 stops growing and decreases rapidly. The positions of all three peaks have a similar trend to the internal resistance. Especially for Cell 02, the significant increase in internal resistance in the first 2000 cycles causes the peaks to shift toward higher voltages. No LAM at the PE is inferred from ICA.

For Cell 03, as a retired battery, its Peak 3 does not increase initially but decreases linearly and rapidly until it disappears. The disappearance of Peak 3 coincides with the onset of a slow change in the intensity of Peak 2, implying an adequate lithium inventory. However, the high temperature between 9680 and 10,160 cycles destabilizes the SEI film on graphite, and the film continuously breaks down and reforms, contributing to LLI and a rapid capacity decline after 10,000 cycles [33,34]. Moreover, the shift in Peak 1 indicates that the LLI is accompanied by the LAM of the PE.

### 3.2. BYD Battery Module Test Results

#### 3.2.1. Module Capacity before and after Balancing

Figure 6 presents the capacities of the four modules before and after balancing. The initial capacities of the four battery modules are 68.2%, 67.3%, 53.9%, and 53.4%, respectively. We assume that the estimated cycle number of the batteries in their first-life use is approximately 1800 (5 years × 365 cycles/year), and the battery cell capacity degradation speed ranges between 8.5% and 15.8% per 1000 cycles.

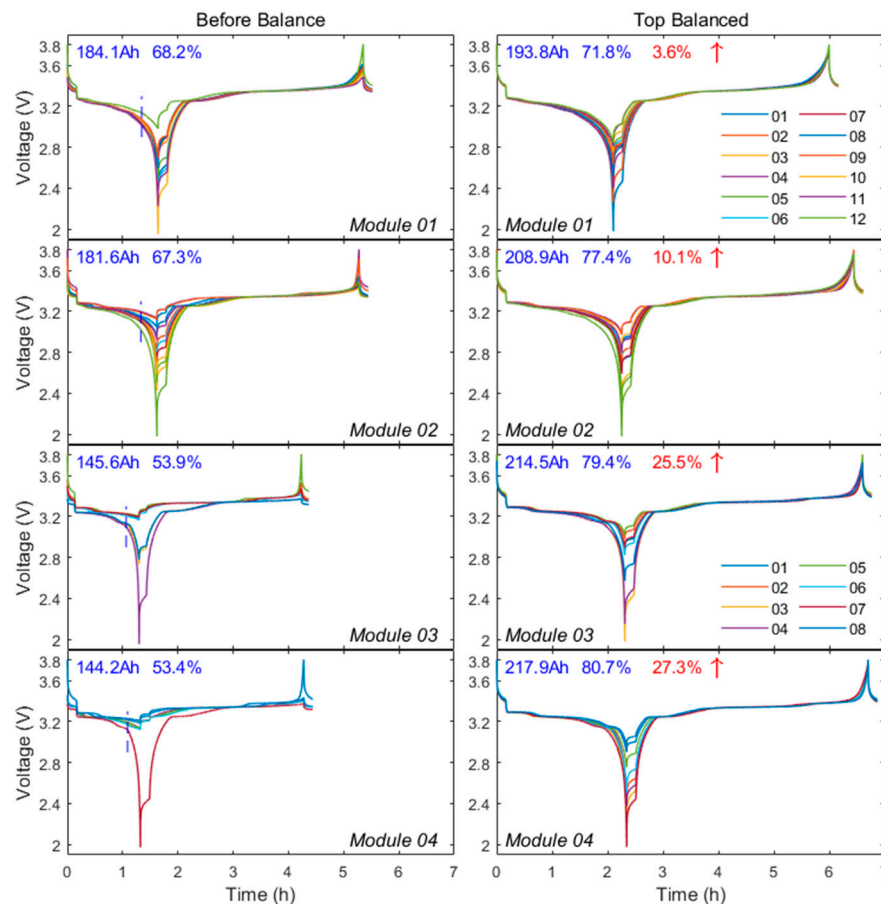


Figure 6. BYD battery module test comparison before and after balancing.

Through the balancing process, their capacities are recovered by 3.6%, 10.1%, 25.5%, and 27.3%, respectively. When breaking down the capacity loss, Modules 03 and 04 exhibit more severe balance issues upon retirement compared to Modules 01 and 02. Module 01 lost 31.8% of its capacity, with 28.2% due to battery cell degradation and 3.6% due to balance issues. Module 02 lost 32.7% of its capacity, with 22.6% due to battery cell degradation and 10.1% due to balance issues. Module 03 lost 46.1% of its capacity, with 20.6% due to battery cell degradation and 25.5% due to balance issues. Module 04 lost 46.6% of its capacity, with 19.3% due to battery cell degradation and 27.3% due to balance issues.

Although the BYD BMS is equipped with a passive balance system, Modules 03 and 04 still exhibited severe balance issues, suggesting that the passive balance system cannot effectively balance the LFP battery pack. In other words, with an effective balance system, the capacities of Modules 03 and 04 could be recovered to about 80%, allowing the battery pack to function for three more years before the capacity drops to 70%.

### 3.2.2. Analysis of Cell Health Conditions

Figure 7 shows the distribution of the cell capacity, voltage, ohmic resistance  $R_0$ , and diffusion resistance  $R_1$  in each module. The values of  $R_0$  and  $R_1$  at about 35% SoC are used for comparison. The maximum and minimum cell capacities and  $R_0$  values are listed in Table 5. Because the internal resistance of the new BYD battery is unknown, the lowest  $R_0$  and  $R_1$  of all of the battery cells, 0.24 mΩ, is considered the benchmark for comparison.

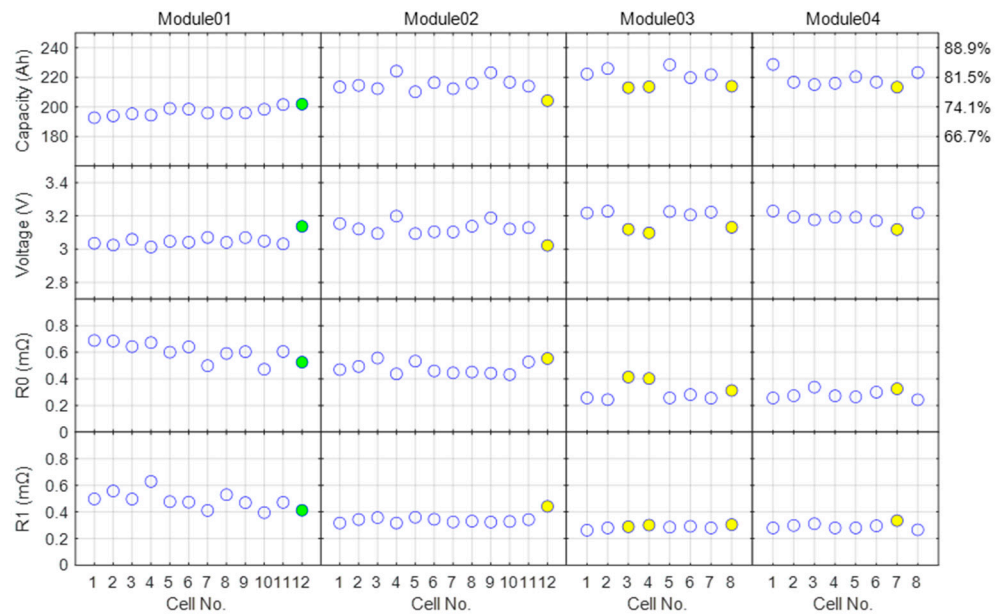


Figure 7. Distribution of cell capacity, voltage, and resistance in each module.

Table 5. BYD battery cell parameter statistics.

Module Number	01	02	03	04
Maximum Cell Capacity	201.9 Ah (74.8%)	224.2 Ah (83.0%)	228.4 Ah (84.6%)	228.7 Ah (84.7%)
Minimum Cell Capacity	193.2 Ah (71.5%)	206.2 Ah (76.4%)	213.5 Ah (79.1%)	215.3 Ah (79.8%)
Capacity Difference	8.7 Ah (3.2%)	18.0 Ah (6.7%)	15.0 Ah (5.5%)	13.4 Ah (5.0%)
Maximum $R_0$ (mΩ)	0.67	0.55	0.40	0.33
Minimum $R_0$ (mΩ)	0.46	0.41	0.24	0.24

In terms of cell capacities, Module 03 and Module 04 have the highest values, followed by Module 02, and Module 01 has the lowest values. The cell capacity difference in a battery module ranges from 3.2% to 6.7%. Regarding the internal resistance, Module 01 has the highest, followed by Module 02 and Module 03, and Module 04 has the lowest. The

difference in internal resistance ranges from 30% to 60%. Higher internal resistance leads to reduced round-trip energy efficiency. For example, the round-trip energy efficiency of Module 04-Cell 01 (the best battery cell) is about 95.9% at 0.25 C charging and 0.5 C discharge currents, which is normal. The internal resistance of Module 01-Cell 01 (the worst battery cell) increases to 2.81 times the lowest value, reducing the round-trip energy efficiency to 92.6%, which is considerably low.

Additionally, Figure 7 shows that the internal resistance of BYD batteries has a negative correlation with the capacity. Cells with a lower SoC have lower capacity and vice versa. For example, Cell 12 in Module 01 has the highest SoC, the highest capacity, and the lowest internal resistance. In Module 03, the SoC of Cells 03, 04, and 08 is obviously lower than that of other cells, with correspondingly lower capacity and higher internal resistance.

From the cell perspective, Module 01 is in the worst health condition since its cells have the lowest capacity and the highest internal resistance. The health condition of Module 02 is better than that of Module 01. The cells in Modules 03 and 04 have the highest capacity and lowest internal resistance. However, due to the balance issues, the available capacity of Modules 03 and 04 is lower. Therefore, Modules 03 and 04 are less used than Modules 01 and 02, resulting in the slower degradation of the batteries.

### 3.2.3. Development of Balance Issues

Multiple factors contribute to the development of LFP battery balance issues, including differences in their internal resistance, temperature, and Coulomb efficiency. During the charging process, higher internal resistance results in a higher voltage and increased heat generation. A higher voltage and temperature facilitate side reactions in the batteries, slightly reducing the Coulomb efficiency and consequently causing SoC variance and balance issues. In addition, LFP battery modules in EVs can experience significant state of charge (SoC) estimation uncertainties due to their voltage characteristics. These uncertainties lead to frequent balance issues [35].

After production, battery cells are tested for their capacity and internal resistance, and only cells with similar values are placed in the same battery pack. Thus, new battery packs usually have good parameter consistency, and balance issues develop slowly in the first few hundred cycles over 2 to 3 years. While an ideally designed balancing system should theoretically achieve near-perfect balance at the end of every full charge event, practical challenges such as cell aging, variations in internal resistance, and operational temperature differences can lead to imbalances that necessitate more frequent correction. This suggests that the current BYD balancing system, although effective under certain conditions, may require further optimization to address these challenges more robustly over the extended lifetime of the battery pack.

In aged LFP battery packs with existing internal resistance differences, balance issues re-emerge faster than in new packs, even after rebalancing. Balance issues become more pronounced as the battery pack ages and require periodic intervention, often more frequently than once a year, especially in second-life applications. This poses a challenge when using second-life LFP batteries in battery energy storage systems (BESSs), highlighting the need for a more effective balance system.

### 3.3. Second-Life Evaluation of the LFP Batteries

Although the BYD and CALB batteries are both LFP batteries, they exhibit different aging characteristics. BYD batteries have a higher energy density of 116 Wh/kg compared to CALB batteries' 100 Wh/kg, but this comes at the cost of inferior aging performance. When the BYD battery's capacity degrades to 70%, the internal resistance increases to at least 2.8 times the benchmark, and the energy efficiency drops to 92.6%. However, CALB batteries maintain consistently low internal resistance until the capacity degrades to 60%. For example, despite the capacity of Cell 03 degrading to 60%, it still shows decent performance, and the round-trip energy efficiency is 94.5% at a 0.5 C current. An abundant electrolyte is crucial in ensuring a long battery cycle life and low internal resistance. How-

ever, increasing the energy density of LFP batteries will result in using less electrolyte, thereby reducing the battery's aging performance.

For the second-life usage of CALB batteries, if the working voltage range remains between 2.80 V and 3.55 V (10%~90% SoC), and high working temperatures are avoided, the charge current is 0.5 C, and the discharge current is 1 C, CALB batteries can have long life cycles. The aging speed of LFP batteries in their second life is expected to be 2% to 4% per 1000 aging cycles. If the batteries are repurposed at 80% SoH, they can be used for 5000 to 10,000 cycles before their capacity degrades to 60%, with an estimated second life of 14 to 28 years, assuming one charge and discharge cycle per day. Even when the capacity degrades below 60%, the battery remains still usable with lower currents.

Although LFP battery cells have a very long cycle life, balance issues remain a significant challenge for LFP battery packs. These issues can induce severe pack capacity reductions. In this study, the useful capacity of the four battery modules could be recovered to 71~80% if properly balanced. Assuming that the battery aging speed for second life can be maintained below 4% per 1000 cycles, the estimated second life of the battery modules is 5000 to 7500 cycles before the capacity drops to 50%. If the battery is charged once daily, it can operate for 14 to 20 years.

#### 4. Morphology Characterization

Two CALB cells, Cell 03 (with 50% capacity) and Cell 05 (with 88% SoH), were disassembled for material analysis. A QUANTA FEG 450 scanning electron microscope (SEM) was employed to examine the material morphology at the micrometer scale, utilizing an accelerating voltage of 20 kV. The SEM imaging was conducted under vacuum conditions.

Figure 8 presents the macroscope and SEM images of the positive and negative electrode materials of the two cells. A visual analysis of Cells 03 and 05 in Figure 8a reveals no surface deposits or mechanical changes to the positive electrode between the two cells. In contrast, a dark grey deposit on the separator at the graphite side is found in Cell 03 but not in Cell 06, indicating the exfoliation of the negative electrode materials.

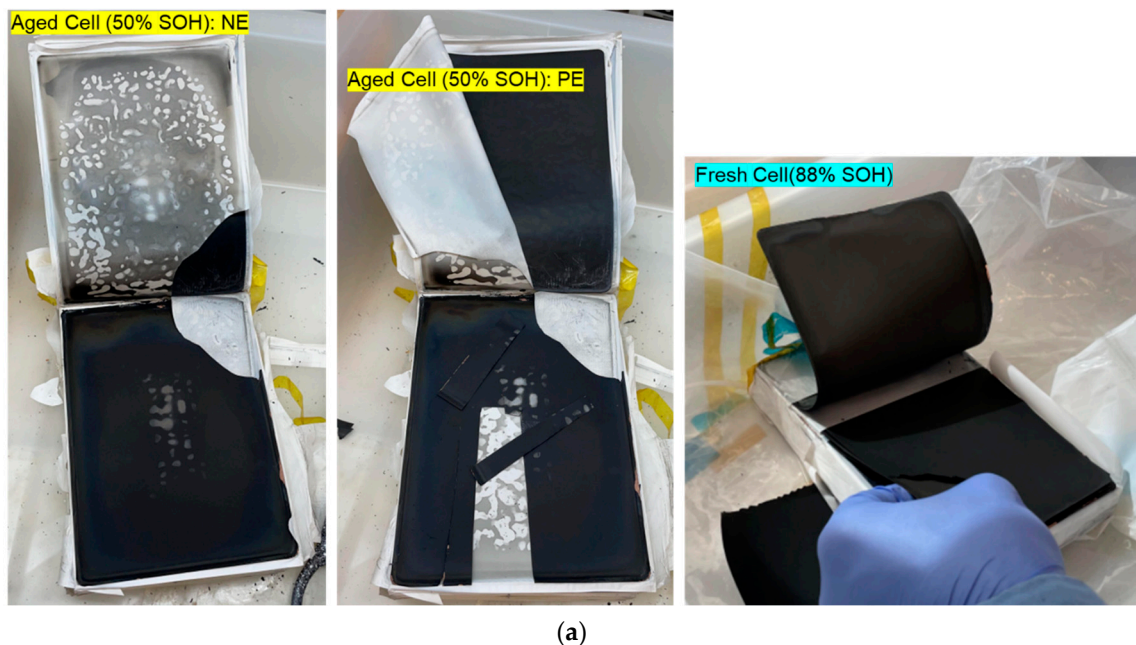
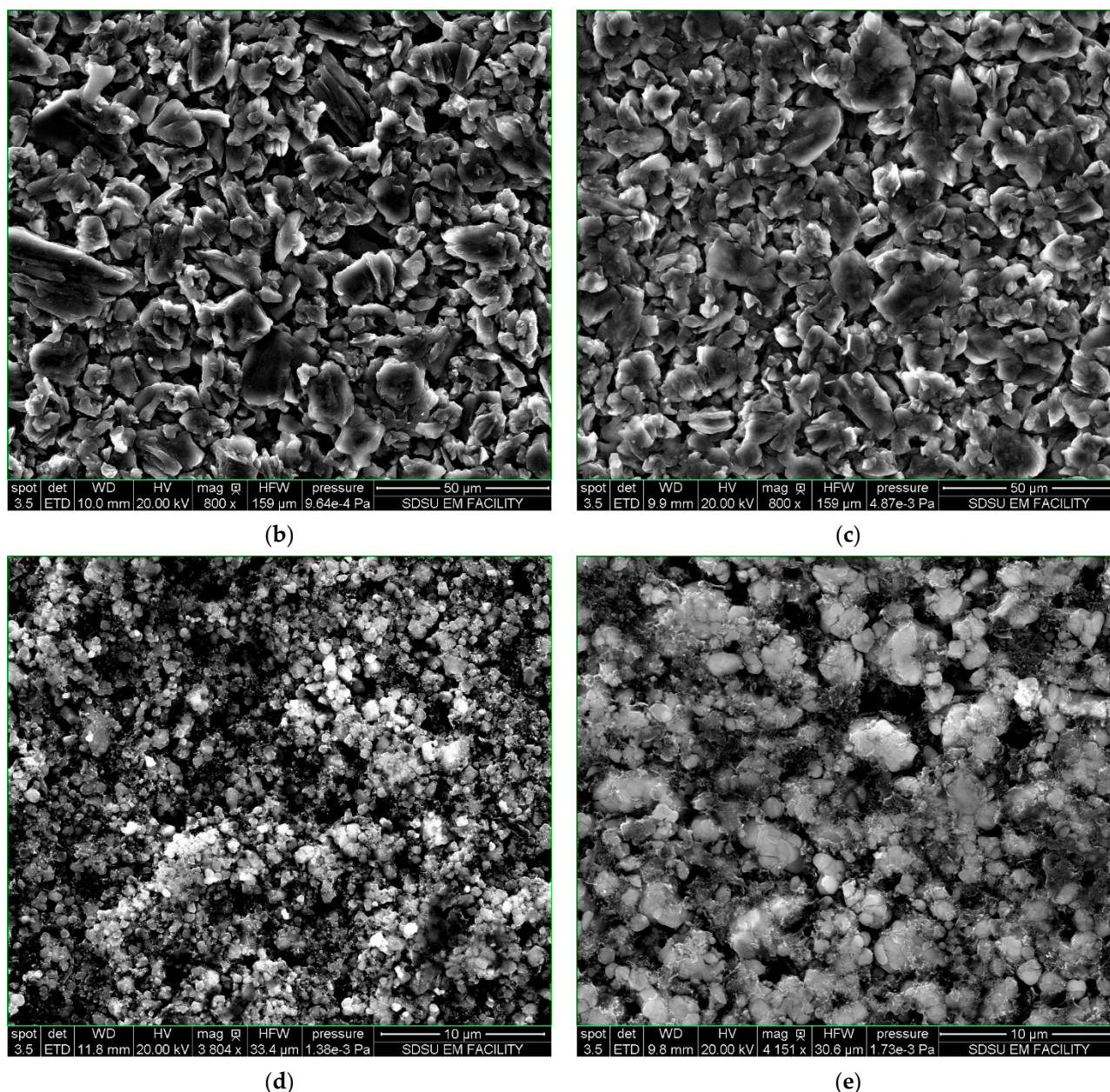


Figure 8. Cont.



**Figure 8.** Post-mortem analysis of two CALB LFP cells. (a) The macroscopic analysis of the PE and NE materials; (b) the SEM image of the fresh cell's graphite electrode; (c) the SEM image of the aged cell's graphite electrode; (d) the SEM image of the fresh cell's positive electrode; (e) the SEM image of the aged cell's positive electrode.

In Figure 8b, the edges of the fresh graphite flakes are slightly more angular compared to those in Figure 8c, which show smoother and more rounded edges. The surface layer is inferred to be SEI reformed in high-temperature cycles at the expense of the lithium inventory. The LFP particles of the fresh electrode in Figure 8d are generally smaller than those of the aged electrode in Figure 8e, and some cracking is visible in the LFP particles of the aged electrode. The high temperatures cause the LFP particles to crack and subsequently aggregate, leading to a reduction in surface area and decreased electrochemical activity. These agglomerates are responsible for the LAM of the PE and the increase in the internal resistance. These findings agree with those in the literature [36,37].

The post-mortem analysis aligns with the aging modes revealed by ICA, indicating that LAM and LLI contribute to the capacity fade during cycling.

## 5. Conclusions

This work conducted two case studies on retired LFP batteries at the cell and module levels, aiming to specify the aging performance of the battery cells, assess the health conditions of the battery modules, and evaluate their second-life potential. The key findings of this study include the following.

1. LFP battery cells have a very long cycle life. For example, Cell 01 loses 33.9% of its capacity after 10,000 aging cycles, with an aging rate of only 3.26% per 1000 cycles.
2. The battery cells' impedance did not increase in the first 10,000 cycles, which is impressive.
3. For second-life use, if the working voltage range remains between 2.80 V and 3.55 V (10~90% SoC), and high working temperatures are avoided, the charge current is 0.5 C, and the discharge current is 1 C, CALB batteries can exhibit very stable aging performance and achieve sustainable and efficient second-life use.
4. High temperatures induce battery aging knee and cause an impedance increase.
5. LFP batteries generally exhibit excellent performance at the cell level, as demonstrated by the CALB 100 Ah cells. However, the BYD module encounters balancing issues at the pack level, making an effective balancing system essential for LFP batteries.

In summary, this study clarified the prospects for the second-life utilization of LFP batteries and proposed strategies to ensure their long second life and performance. It provides recommendations for both the first-life and second-life operation of EV batteries.

**Author Contributions:** Conceptualization, C.M. and W.G.; methodology, W.G. and C.M.; software, W.G. and Z.C.; validation, W.G., Y.F., Z.C., C.T. and J.G.; formal analysis, W.G. and Z.C.; investigation, W.G.; resources, C.M. and J.G.; data curation, W.G., Y.F. and Z.C.; writing—original draft preparation, Z.C. and W.G.; writing—review and editing, Z.C., C.M. and N.V.K.; visualization, Z.C., C.T. and W.G.; supervision, C.M.; project administration, C.M.; funding acquisition, C.M. All authors have read and agreed to the published version of the manuscript.

**Funding:** This research was funded by the California Energy Commission, grant number EPC-19-053.

**Data Availability Statement:** Data are available on request from the corresponding author.

**Conflicts of Interest:** The authors declare no conflicts of interest.

## References

1. King, N. EVs Forecast to Account for Two Thirds of Global Light-Vehicle Sales in 2035. Available online: <https://ev-volumes.com/news/ev/evs-forecast-to-account-for-two-thirds-of-global-light-vehicle-sales-in-2035/> (accessed on 29 July 2024).
2. Hu, X.; Deng, X.; Wang, F.; Deng, Z.; Lin, X.; Teodorescu, R.; Pecht, M.G. A Review of Second-Life Lithium-Ion Batteries for Stationary Energy Storage Applications. *Proc. IEEE* **2022**, *110*, 735–753. [\[CrossRef\]](#)
3. Gao, W.; Cao, Z.; Kurdkandi, N.V.; Fu, Y.; Mi, C. Evaluation of the Second-Life Potential of the First-Generation Nissan Leaf Battery Packs in Energy Storage Systems. *eTransportation* **2024**, *20*, 100313. [\[CrossRef\]](#)
4. Yang, X.-G.; Leng, Y.; Zhang, G.; Ge, S.; Wang, C.-Y. Modeling of Lithium Plating Induced Aging of Lithium-Ion Batteries: Transition from Linear to Nonlinear Aging. *J. Power Sources* **2017**, *360*, 28–40. [\[CrossRef\]](#)
5. Hossain, E.; Murtaugh, D.; Mody, J.; Faruque, H.M.R.; Sunny, H.M.S.; Mohammad, N. A Comprehensive Review on Second-Life Batteries: Current State, Manufacturing Considerations, Applications, Impacts, Barriers & Potential Solutions, Business Strategies, and Policies. *IEEE Access* **2019**, *7*, 73215–73252. [\[CrossRef\]](#)
6. Hua, Y.; Liu, X.; Zhou, S.; Huang, Y.; Ling, H.; Yang, S. Toward Sustainable Reuse of Retired Lithium-Ion Batteries from Electric Vehicles. *Resour. Conserv. Recycl.* **2021**, *168*, 105249. [\[CrossRef\]](#)
7. Nitta, N.; Wu, F.; Lee, J.T.; Yushin, G. Li-Ion Battery Materials: Present and Future. *Mater. Today* **2015**, *18*, 252–264. [\[CrossRef\]](#)
8. Ohneseit, S.; Finster, P.; Floras, C.; Lubenau, N.; Uhlmann, N.; Seifert, H.J.; Ziebert, C. Thermal and Mechanical Safety Assessment of Type 21700 Lithium-Ion Batteries with NMC, NCA and LFP Cathodes—Investigation of Cell Abuse by Means of Accelerating Rate Calorimetry (ARC). *Batteries* **2023**, *9*, 237. [\[CrossRef\]](#)
9. Sockeel, N.; Gafford, J.; Manjrekar, M.; Mazzola, M. Economic Analysis of High-Longevity Battery Capacity Fades for Electric Vehicles Supercharger Buffering Application. *IEEE Trans. Transp. Electrification* **2020**, *6*, 995–1002. [\[CrossRef\]](#)
10. Gao, W.; Cao, Z.; Fu, Y.; Turchiano, C.; Kurdkandi, N.V.; Gu, J.; Mi, C. Comprehensive Study of the Aging Knee and Second-Life Potential of the Nissan Leaf E+ Batteries. *J. Power Sources* **2024**, *613*, 234884. [\[CrossRef\]](#)
11. Attia, P.M.; Bills, A.; Planella, F.B.; Dechent, P.; dos Reis, G.; Dubarry, M.; Gasper, P.; Gilchrist, R.; Greenbank, S.; Howey, D.; et al. Review—“Knees” in Lithium-Ion Battery Aging Trajectories. *J. Electrochem. Soc.* **2022**, *169*, 060517. [\[CrossRef\]](#)

12. Safari, M.; Delacourt, C. Aging of a Commercial Graphite/LiFePO<sub>4</sub> Cell. *J. Electrochem. Soc.* **2011**, *158*, A1123. [[CrossRef](#)]
13. Sun, S.; Guan, T.; Shen, B.; Leng, K.; Gao, Y.; Cheng, X.; Yin, G. Changes of Degradation Mechanisms of LiFePO<sub>4</sub>/Graphite Batteries Cycled at Different Ambient Temperatures. *Electrochim. Acta* **2017**, *237*, 248–258. [[CrossRef](#)]
14. Naumann, M.; Spingler, F.B.; Jossen, A. Analysis and Modeling of Cycle Aging of a Commercial LiFePO<sub>4</sub>/Graphite Cell. *J. Power Sources* **2020**, *451*, 227666. [[CrossRef](#)]
15. Dubarry, M.; Liaw, B.Y. Identify Capacity Fading Mechanism in a Commercial LiFePO<sub>4</sub> Cell. *J. Power Sources* **2009**, *194*, 541–549. [[CrossRef](#)]
16. Dubarry, M.; Truchot, C.; Liaw, B.Y. Cell Degradation in Commercial LiFePO<sub>4</sub> Cells with High-Power and High-Energy Designs. *J. Power Sources* **2014**, *258*, 408–419. [[CrossRef](#)]
17. Jiang, Y.; Jiang, J.; Zhang, C.; Zhang, W.; Gao, Y.; Li, N. State of Health Estimation of Second-Life LiFePO<sub>4</sub> Batteries for Energy Storage Applications. *J. Clean. Prod.* **2018**, *205*, 754–762. [[CrossRef](#)]
18. Simolka, M.; Heger, J.-F.; Traub, N.; Kaess, H.; Friedrich, K.A. Influence of Cycling Profile, Depth of Discharge and Temperature on Commercial LFP/C Cell Ageing: Cell Level Analysis with ICA, DVA and OCV Measurements. *J. Electrochem. Soc.* **2020**, *167*, 110502. [[CrossRef](#)]
19. Wheeler, W.; Bultel, Y.; Venet, P.; Sari, A.; Riviere, E. Postmortem Analysis of 18650 Graphite/LFP Cells in a Long-Term Aging Study for Second-Life Applications. *Batteries* **2024**, *10*, 119. [[CrossRef](#)]
20. Zhu, Y.; Zhu, J.; Jiang, B.; Wang, X.; Wei, X.; Dai, H. Insights on the Degradation Mechanism for Large Format Prismatic Graphite/LiFePO<sub>4</sub> Battery Cycled under Elevated Temperature. *J. Energy Storage* **2023**, *60*, 106624. [[CrossRef](#)]
21. Etxandi-Santolaya, M.; Canals Casals, L.; Corchero, C. Extending the Electric Vehicle Battery First Life: Performance beyond the Current End of Life Threshold. *Heliyon* **2024**, *10*, e26066. [[CrossRef](#)]
22. Ramirez-Meyers, K.; Rawn, B.; Whitacre, J.F. A Statistical Assessment of the State-of-Health of LiFePO<sub>4</sub> Cells Harvested from a Hybrid-Electric Vehicle Battery Pack. *J. Energy Storage* **2023**, *59*, 106472. [[CrossRef](#)]
23. Jiang, Y.; Jiang, J.; Zhang, C.; Zhang, W.; Gao, Y.; Guo, Q. Recognition of Battery Aging Variations for LiFePO<sub>4</sub> Batteries in 2nd Use Applications Combining Incremental Capacity Analysis and Statistical Approaches. *J. Power Sources* **2017**, *360*, 180–188. [[CrossRef](#)]
24. CALB CA100 3.2V 100Ah LiFePO<sub>4</sub> Lithium Ion Battery—LiFePO<sub>4</sub> Battery. Available online: <https://www.lifepo4-battery.com/Products/CALB-Battery/CALB-CA100-100Ah.html> (accessed on 26 July 2024).
25. Hu, X.; Li, S.; Peng, H. A Comparative Study of Equivalent Circuit Models for Li-Ion Batteries. *J. Power Sources* **2012**, *198*, 359–367. [[CrossRef](#)]
26. Wang, X.; Wei, X.; Zhu, J.; Dai, H.; Zheng, Y.; Xu, X.; Chen, Q. A Review of Modeling, Acquisition, and Application of Lithium-Ion Battery Impedance for Onboard Battery Management. *eTransportation* **2021**, *7*, 100093. [[CrossRef](#)]
27. Gao, W.; Zou, Y.; Sun, F.; Hu, X.; Yu, Y.; Feng, S. Data Pieces-Based Parameter Identification for Lithium-Ion Battery. *J. Power Sources* **2016**, *328*, 174–184. [[CrossRef](#)]
28. Dubarry, M.; Anseán, D. Best Practices for Incremental Capacity Analysis. *Front. Energy Res.* **2022**, *10*, 1023555. [[CrossRef](#)]
29. Dubarry, M.; Liaw, B.Y.; Chen, M.-S.; Chyan, S.-S.; Han, K.-C.; Sie, W.-T.; Wu, S.-H. Identifying Battery Aging Mechanisms in Large Format Li Ion Cells. *J. Power Sources* **2011**, *196*, 3420–3425. [[CrossRef](#)]
30. Dubarry, M.; Truchot, C.; Liaw, B.Y. Synthesize Battery Degradation Modes via a Diagnostic and Prognostic Model. *J. Power Sources* **2012**, *219*, 204–216. [[CrossRef](#)]
31. Dubarry, M.; Beck, D. Perspective on Mechanistic Modeling of Li-Ion Batteries. *Acc. Mater. Res.* **2022**, *3*, 843–853. [[CrossRef](#)]
32. Anseán, D.; Dubarry, M.; Devie, A.; Liaw, B.Y.; García, V.M.; Viera, J.C.; González, M. Operando Lithium Plating Quantification and Early Detection of a Commercial LiFePO<sub>4</sub> Cell Cycled under Dynamic Driving Schedule. *J. Power Sources* **2017**, *356*, 36–46. [[CrossRef](#)]
33. Andersson, A.M.; Edström, K. Chemical Composition and Morphology of the Elevated Temperature SEI on Graphite. *J. Electrochem. Soc.* **2001**, *148*, A1100. [[CrossRef](#)]
34. Guo, Z.; Chen, Z. High-Temperature Capacity Fading Mechanism for LiFePO<sub>4</sub>/Graphite Soft-Packed Cell without Fe Dissolution. *J. Electroanal. Chem.* **2015**, *754*, 148–153. [[CrossRef](#)]
35. Halfi, I. NMC vs LFP: Safety and Performance in Operation. Available online: <https://powerup-technology.com/nmc-vs-lfp-safety-and-performance-in-operation/> (accessed on 29 July 2024).
36. Liu, P.; Wang, J.; Hicks-Garner, J.; Sherman, E.; Soukiazian, S.; Verbrugge, M.; Tataria, H.; Musser, J.; Finamore, P. Aging Mechanisms of LiFePO<sub>4</sub> Batteries Deduced by Electrochemical and Structural Analyses. *J. Electrochem. Soc.* **2010**, *157*, A499. [[CrossRef](#)]
37. Simolka, M.; Heger, J.-F.; Kaess, H.; Biswas, I.; Friedrich, K.A. Influence of Cycling Profile, Depth of Discharge and Temperature on Commercial LFP/C Cell Ageing: Post-Mortem Material Analysis of Structure, Morphology and Chemical Composition. *J. Appl. Electrochem.* **2020**, *50*, 1101–1117. [[CrossRef](#)]

**Disclaimer/Publisher’s Note:** The statements, opinions and data contained in all publications are solely those of the individual author(s) and contributor(s) and not of MDPI and/or the editor(s). MDPI and/or the editor(s) disclaim responsibility for any injury to people or property resulting from any ideas, methods, instructions or products referred to in the content.